THE EFFECTS OF SIZE DISTRIBUTION OF GOLD NANOPARTICLES ON NANOSPRINGS FORMATION AND PROCESS EFFICIENCY

A Thesis

in Partial Fulfilment of the Requirements for the

Degree of Master of Science

with a

Major in Physics

in the

College of Graduate Studies

University of Idaho

by

Nawal Alsaiari

Major Professor: David N. Mcllroy, PhD.

Committee Members: Leah Bergman, PhD., Matthew M. Hedman, Ph.D.

Department Administrator: Ray Von Wandruszka, Ph.D.

December 2017

Authorization to Submit Thesis

The thesis of Nawal Mabkhoot Alsaiari, submitted for the degree of Master of Science with a Major in Physics and titled, "THE EFFECTS OF SIZE DISTRIBUTION OF GOLD NANOPARTICLES ON NANOSPRINGS FORMATION AND PROCESS EFFICIENCY," has been reviewed in final form. Permission, as indicated by the signatures and dates given below, is now granted to submit final copies to the College of Graduate Studies for approval.

Major Professor: _____ Date: _____

David N. McIlroy, Ph.D.

Committee Members: _____ Date: _____

Leah Bergman, Ph.D.

_____ Date: _____

Matthew M. Hedman, Ph.D.

Department Administrator: _____ Date: _____

Ray Von Wandruszka, Ph.D.

Abstract

Gold nanoparticles are examined due to their unique optical properties, which make them advantageous for various applications. In this study, Gold nanoparticles were synthesized by reduction reaction method between chloroauric acid ($HAuCl_4$) and trisodium citrate ($Na_3\ C_6\ H_5\ O_7$). These two agents, gold chloride concentration and trisodium citrate concentration, were changed while the other experimental parameters such as temperature and mixing rate were kept at the same level, which effect both particles' size and size distributions directly. The size and the shape of gold particles can be characterized by using scanning electron microscopy (SEM). The particles' sizes can be produced in a range of 0.99 to 5.3 μm, and these particles have a spherical shape. In addition, the UV-visible spectroscopy was used in this study to investigate the effect of various diameters of gold nanoparticles on the surface plasmon resonance. Also, the vapor liquid solid method was utilized to explore the range of sizes of Au NPs that most efficiently produces nanosprings.

Keywords:

Gold nanoparticles; Citrate reduction reaction; Surface plasmon resonance; Silica nanosrings;

Acknowledgments

I would like to express my grateful thanks to everyone who contributed to make this thesis completed. First of all, I sincerely thank my academic advisor, Professor David N. McIlroy, for his guidance and encouragement through working in his group. Besides that, I would like to thank Dr. Leah Bergman, and Dr. Matthew M. Hedman for being my committee members. Last but not the least, I am very thankful to Negar Rajabi and Marshall Boyland for their assistance during the period of my project work.

Dedication

I dedicate this work to the first and the most important man and woman in my life, my parents, my supportive siblings, and my lovely friends for the inspiration and encouragement they gave me to complete this degree.

Table of Contents

List of Figures

List of Tables

CHAPTER 1: Introduction

Gold is considered as one of the first metals reported to have been discovered with reports of its use dating back to several thousands of years. Colloidal gold, assumed to be suspended gold nanoparticles can be found in books and articles by ancient Chinese, Indian, and Arabian scientists from the 5 – 4th century BC. Their importance in medicine has been well documented by these ancient researchers [8]. During the Middle Ages, the usage of gold nanoparticles was extensively researched by several alchemists who obtained this colloidal gold by reducing gold chloride with vegetable extracts in suitable solvents. Medieval scientists used gold to treat mental illnesses, syphilis, leprosy, the plague, etc. and was even considered the elixir of longevity by the French. The first ever book on the importance of colloidal gold was published by Francisco Antonii in 1618 and this documented the medicinal and practical uses of gold nanoparticles [8].

Nanomaterials with diameters smaller than 100 nm are considered as nanoparticles. Among these, gold nanoparticles (Au NPs) are popular because their optical properties can be easily tuned which is useful for applications like biosensing [30], bioimaging [33], catalysis [7], etc. Research for developing new methods for synthesizing functionalized gold nanoparticles and using them for different applications is currently a popular topic. There are regular developments in gold nanoparticle synthesis recipes with focus on the control over their size and shape. Apart from sensing, gold nanoparticles are also used for different photothermal and drug delivery applications [12, 4]. In this way, the control in the structural properties of gold nanoparticles will keep on being used in devices for novel future applications.

Au NPs are a reliable and interesting class of materials used widely in biosensing and many research groups have shown that they can be utilized as other kinds of sensors also for testing biological and chemical samples [5, 16, 28]. Besides, there are some problems that need to be taken care of before colloidal Au NPs can be effectively used in medical applications. This consists of the reproducibility, dependability, versatility in fabricating Au NPs-based devices that lasts for a long time. Soon, we imagine that the multidisciplinary research will give new important knowledge into the Au NPs-based nanotechnology.

It is interesting to focus on gold nanoparticles because monodispersed colloids can be prepared through simple synthesis techniques [11] such as the Turkevich method, emulsion polymerization method, thiol, etc. As first recommended by Wessel, Au nanoparticles are very interesting to study since they absorb incident electromagnetic radiation and increase the overall electromagnetic wave by many orders of intensity [42]. This increase in electromagnetic field is due to the surface plasmon resonance that gold nanoparticles go through when they absorb radiation. When incident electromagnetic radiation strikes the surface of the gold nanoparticles, localized surface plasmons in the metal are excited that result in the enhancement of the overall wave. The highest enhancement in the field takes place when the frequency of the incident radiation in the same as the plasmon resonance frequency. This field enhancement happens when the oscillation of the localized surface plasmons are perpendicular to the metal surface [42]. Thus, colloidal metal nanoparticles of gold and silver especially with rough surfaces are used extensively to increase the overall field of the incident electromagnetic radiation.

1.2. Different Shapes of Gold Nanoparticles:

Gold nanoparticles can be produced in different shapes. The first shape of gold nanoparticles is the gold nanorod, which is synthesized through the template method and produced by the electrochemical deposition of gold [38]. The other shape is gold nanocage, which is formed through the galvanic replacement reaction between truncated silver nanocubes and aqueous $HAuCl_4$. The gold nanospheres are produced by the reduction of an aqueous $HAuCl_4$ using citrate as a reducing agent. Gold nanoshells which use surface plasmon resonance peaks (ranging from visible to near I.R. region) for the designing and manufacture. The center of gold nanoshells is created of silica and the external surface is created of gold [38]. Therefore, various shapes of Au NPs are prepared from various methods.

1.3. Properties of Different Shapes of Gold Nanoparticles:

The shape and size of gold nanoparticles determine the optical properties of the nanoparticles. Spherical shaped colloidal golds have absorption maxima between 523 nm and the near infrared part of the spectrum [17]. In another hand, the SPR wavelength is about 300 nm for gold nanoshell's thickness from 5 to 20 nm, and it depends on the shell thickness. However, gold nanorods have an absorption maxima of about 800 nm. Besides that, gold nanocage absorption appears around 800 nm for Au NPs cell size around 50 nm. The difference in the absorption properties of the different shapes is caused by the anisotropic distribution of surface electrons [9].

1.4. Optical Properties of Gold Nanoparticles

1.4.1. The Surface Plasmon Resonance Interests:

The area of Au NPs research has encountered significant consideration because of their extraordinary optical properties. The different optical properties of Au NPs are because of their size and shape differences which give new electronic and optical properties. A particular highlight of Au NPs is the strong color in their suspended form due to the surface plasmon resonance (SPR) [21,22]. This means that a certain part of the wavelength in the visible region will be absorbed by the Au NPs, while they reflect another part of it. The reflected wavelength is responsible for the material color. Nanoparticles with smaller dimensions absorb the blue-green region of the spectrum (400-500 nm) while red light (~700 nm) is reflected. This results in the deep red color of colloidal Au NPs [21,22].

1.4.2. How the Surface Plasmon Resonance Band is Formed:

Au NPs were employed as colouring agents for recolouring stained glass on churches going back to the seventeenth century [46,10]. The recoloured glasses with Au NPs are ruby red. The reason for the color of colloidal Au NP samples was given by Mie who figured out Maxwell's equations for the absorption and scattering of electromagnetic radiation by spherical particles. Mie’s theory is generally used to ascertain the electronic spectra if the material dielectric is known. The absorption wavelength of Au NPs is because of the coherent oscillation of the conduction band electrons prompted by the electromagnetic field. This is known as surface plasmon resonance and this phenomenon is observed in nano as well as bulk Au [46,10].

For a given spherical metal nanoparticle of radius, R, Mie's theory for the extinction cross section (absorption + scattering), (σext), when the wavelength of light causing the excitation of these nanoparticles greatly exceeds that of the particles, is denoted by:

$$\sigma_{ext}(\omega) = 9\,\frac{\omega}{c}\,\varepsilon_m^{\frac{3}{2}}\,V_o\,\frac{\varepsilon_2(\omega)}{[\varepsilon_1\,(\omega)+2\varepsilon_m]^2+\varepsilon_2\,(\omega)^2} \qquad 1$$

"where Vo = $(4\pi/3)R^3$, ω is the angular frequency of the excitation frequency, ε_m the dielectric function of the medium surrounding the metallic nanoparticles. ε_1 and ε_2 correspond to the real and imaginary parts of the dielectric function of the metallic nanoparticles respectively" [35,50].

The existence of surface absorption is depicted in equation 1 when $\varepsilon_1(\omega) \approx -2\varepsilon_m$ only when it is ε_2 valid for slight or weak dependence of ω. Typically, strong colors are not observed in metals such as In, Sn and Cd because their plasma frequencies are in the end of UV range of the spectrum. However, in the case of "coinage metals", their plasma frequencies are in the visible portion of the spectrum as a result of their conduction band transition. Red shift and broadening of electronic absorption spectra resulting from the aggregation state of the nanoparticles is often realised. In this case, Mie's theory's assumption of non-interacting nanoparticles does not hold. Instead near-field coupling between particles that are close together and far-field dipolar coupling are dominant in the spectrum. Plasmonic oscillations of a single nanoparticle induces similar oscillations in adjacent nanoparticles thus creating the dipolar fields [35].

1.4.3. Size verses SPR Band:

The surface plasmon resonance absorption peaks move to lower energy regions with an increase in the particle size. It has been observed that the width and position of the SPR peak increases as the diameter of the Au nanoparticles increase [21]. That is, the peaks get more broad and also redshift towards higher wavelength regions (lower energy) as the size of the nanoparticles increase. The SPR of Au NPs also relies upon the structure, dielectric properties, morphology, and surface functionalization of the particles and refractive index of the suspending medium. For instance, for gold colloidal suspension with diameter of 13 nm, the SPR maxima is around 520 nm, and for 5–6 nm silver NPs, the SPR maxima is about 400 nm. The SPR maxima of the Au NPs can be deliberately tuned by changing the measure of the Au NPs. [21].

1.5. Using Gold Nanoparticle to Grow Nanosprings

Gold nanoparticles employ a significant role as a catalyst to fabricate nanosprings. Nanosprings were developed as a modified form of nanowires that coiled into a helical or spring like form due to different forces acting on the wire in the nanoscale [25, 34]. Specific nanostructures such as nanorods, nanowires, and nanosprings are essential for the fabrication of nanomachines and have significant usability in applications in sensing and fabrication of other nanodevices [34]. Among them, the nanosprings have as of late pulled in much consideration in the nanoscience community. Because of their enhanced structural flexibility and superior material strength, these nanosprings ought to be reasonable for several important applications in electromagnetic sensing and device fabrication [34]. Be that as it may, studying the efficiency of Si nanosprings based on the Au nanoparticles' size employed is an interesting field of study.

1.5.1. Structure of Silica Nanosprings:

Nanosprings are nanowires that are twisted and therefore form a helical structure [43]. Nanospring formation is initiated by the introduction of oxygen in the vapor-liquid-solid (VLS) mechanism. It shows a powerful driving force for the formation of nanosprings from oxidation of the absorbed Silicon by a catalyst [43]. Helical nanosprings is a new family in the family of one-dimensional nanostructures. In addition to their expected structural flexibility, they also exist as an extra opportunity in nanoengineering of parameters such as periodicity and helicity [49]. The helical silica nanostructure can be synthesized additionally through the chemical vapor deposition (CVD) and physical characterization using scanning electron microscopy (SEM), atomic force microscopy (AFM) and transmission electron microscopy (TEM). The silica nanostructure is manufactured to be several microns in length and various nanometres in diameter of variable periodicity [49].

1.5.2. Structural Properties of Silica Nanosprings:

Silica nanosprings are in the shape of a coil, one dimensional and have a gravimetric surface area of $400 m^2/g$ [26]. The nanosprings are unchanged for a temperature up to 1050 °C in humid conditions. In addition, silica nanosprings form a chemical bond at their base to the surface on which they are developed from. Also, under flowing of gas or liquid, nanosprings remain in place during the formation of the chemical bond. The dielectric properties of nanosprings make them desirable in sensor applications. Any kinds of material can coat nanosprings to accomplish a given chemical, reaction, or property [26]. Si nanosprings possess a high flexibility like any spring. When the silica nanospring is bent, it will be under elastic strain and thus a considerable amount of elastic energy will be stored. On the other hand, when the nanospring is straight, it will not store elastic energy [49]. When heat is applied

on the silica nanospring ends, the heated ends will expand while the middle part that is not heated will contract, and thus a deduction that there are highly elastic can be made. Beside the structural flexibility, Si nanosprings also have a variable periodicity. The flexibility and periodicity of nanosprings allow them to be applied in electronic systems, in nanomechanical applications, in composite materials, and in electromagnetic systems. The low thermal expansion and contraction rate of nanosprings make them to be used employed as springs [49].

CHAPTER 2: Materials Preparation

2.1. Materials:

The chemicals employed in this work 24 carat gold (Au), nitric acid (HNO_3) (69.4%), hydrochloric acid (HCl) (37.2%), water (H_2O), trisodium citrate ($Na_3\ C_6\ H_5\ O_7$) (99.8%), methanol(CH_4O) (99.9%), Isopropyl alcohol (C_3H_8O) (99.9%), acetone (C_3H_6O) (99.7%), ethanol (CH_3CH_2OH) (99.9%), and silicon (100) wafers as a support for the Au nanoparticles to grow silica nanosprings.

2.2. Synthesis of gold nanoparticles (Au NPs):

Gold nanoparticles were synthesized using the citrate reduction method, first proposed by Turkevich, Stevenson, and Hillier in 1951, where colloidal gold nanoparticles were prepared by the reduction of chloroauric acid ($HAuCl_4$) using trisodium citrate ($Na_3C_6H_5O_7$). This method produces Au nanoparticles having an average diameter of 200 nm. The method described by Turkevich et al. was an extended version of a recipe proposed by Hauser and Lynn proposed in 1940. This citrate reduction method has also been used to synthesize colloidal silver nanoparticles. Turkevich et al. describes a series of color changes occurring to the solution over a period of time, where a transparent light-yellow solution switched to deep red, which pointed out at the formation of gold nanoparticles [39].

2.2.1. Procedure for production of gold nanoparticles:

In this study, Au NPs were synthesized per the Turkevich and Frens method. The initial tetrachloroauric acid ($HAuCl_4$) was produced by dissolving 5 mg of 24 carat gold in aqua-regia (1:4 mixture of concentration HNO_3 and concentration HCl). This produces a yellow solution. The solvents were evaporated off, leaving a yellow powder of $HAuCl_4$. Next, 50 mg of $HAuCl_4$ was dissolved in 75 mL of distilled water to make a $AuCl_3$ solution. The mixture

was then stirred vigorously while heating to 100 ºC. Simultaneously, 294.1 g/mole (about 3 mole equivalents) of trisodium citrate was dissolved in about 15 mL water and heated to 100 ºC. The citrate solution was then added to Au solution and stirred vigorously using Teflon coated magnetic stirrers for approximately 20 minutes until the solution turned deep red but transparent. The solution was then cooled, and methanol was added in a 1:1 ratio with the solution. The solution turned a deep shade of blue, following which the solution was centrifuged at 3.3k rpm for approximately 10 minutes to separate out the Au NPs. After the particles were centrifuged the supernatant (liquid on top) was decanted off and refilled with methanol. This solution was then sonicated until the particles re-suspended and the solution turned translucent black/deep purple and no particulate suspension is visible. This washing procedure was repeated three times. After decanting off the last portion of methanol used for washing, 5 – 10 mL of methanol was added and sonicated until no particle is visible. This procedure results in gold nanoparticles suspended in a methanol solution.

2.2.2. Calculations for synthesizing different sizes of Au NPs

In this experiment, nine solutions were prepared, and a standard solution was given to see the difference between them. Those solutions have different Au concentrations as well as $AuCl_3$ and trisodium citrate concentrations to investigate the impact of various concentrations on the final particle size distributions. Seven of these nine solutions were made by following the same method for different ratios of the solutions while the eighth and ninth solutions were different. From solutions 1 to 7 the concentrations were increased gradually from 33 mg until 100 mg and from 2 M to 6 M of both $AuCl_3$ and trisodium citrate respectively to have large size of Au nanoparticles. However, for solutions 8 and 9, the concentration of $AuCl_3$ was kept

at the same amount (50 mg) while the trisodium citrate concentration was decreased to 2 and 1 M to obtain small diameter of Au nanoparticle.

Concentration / **solutions**	Mass of Au (mg)	Mass of $AuCl_3$ (mg)	Concentration of trisodium citrate (M)
First solution	3.3	33	2
Second solution	4.17	41.67	2.5
Third solution	5	50	3
Fourth solution	5.8	58.3	3.5
Fifth solution	7	70	4
Sixth solution	8.3	83	5
Seventh solution	10	100	6
Eighth solution	5	50	2
Ninth solution	5	50	1

Table 2.1: Calculations for synthesizing different sizes of Au NPs

CHAPTER 3: Experimental Methods

3.1. Characterization of the AU NPs

3.1.1. Scanning Electron Microscopy

The Scanning Electron Microscopy (SEM) is used to determine the size of Au NPs, and it is also employed to understanding surface morphology and material shapes, especially in nanomaterials. When the sample is subjected to a narrow stream of electrons, auxiliary electrons are radiated from the sample surface. Morphology of the surface can be seen by two-dimensional filtering of the electron beam over the surface and obtaining of a picture from the identified optical electrons [51].

3.1.1.1. SEM working principles

The SEM requires an electron optical framework to deliver an electron beam, a specimen stage to put the specimen on, a secondary electron detector to gather backscattered electrons, an image display unit, and an operation framework to perform different operations [31]. The electron optical framework comprises of an electron gun, a condenser focal point and a target focal point to create an electron beam, an examining loop to check the electron beam, and other optical and electronic components. The electron optical framework (within the magnifying lens segment) and the sample are kept at vacuum [31].

3.1.1.2. Electrons in an SEM

Thermoelectrons are transmitted from a fiber (cathode) made of a thin tungsten wire (about 0.1 mm) by heating the fiber at high temperature (around 2800K). These thermoelectrons are assembled as a beam, streaming into the metal plate (anode) by applying a positive voltage (1 to 30 kV) to the anode. In the event that a gap is made at the focal point of the anode, the electron bar moves through this gap. When you put an anode (called a

Wehnelt electrode) between the cathode and anode and apply a negative voltage to it, you can modify the current of the stream of electrons [31]. Right now, the electron beam is finely engaged by the activity of the Wehnelt cathode. The finest purpose of the beam is called the crossover, and this is viewed as a real electron source with a dimension of 15 to 20 μm [31].

3.1.1.3. Final Image Generation in an SEM

The output signals from the backscattered secondary electron detector are increased and after that exchanged to the computer screen. Since the filtering on the computer screen is synchronized with the electron-probe, variations in brightness, which is a function of the quantity of emitted secondary electrons, appears on the screen, subsequently shaping an SEM image. A cathode-ray tube (CRT) was utilized for a long time as a monitor; however as of late, LCDs have been broadly utilized [31]. All in all, the check speed of the electron scan can be changed in a few stages; an extremely quick output speed is utilized for perception and a moderate output speed is utilized for procurement or sparing of images.

In this study, after preparing gold nanoparticles' solutions, we placed drops of each solution on a substrate individually. The substrate was used here is a silicon wafer, and before using it, it was cleaned thoroughly in acetone and polished by sonicating for about 10 minutes. This washing was also repeated using ethanol, isopropyl alcohol, and deionized water. After the wafer was dried, it was measured to know its mass by using the scale. In that time, the solution was ready to be dried on wafer. After the solution was dried on the wafer, the wafer was remeasured to know the mass of Au NPs. In that moment, we took that silicon wafer to get SEM images to measure the particles' diameter.

3.1.1.4. Measuring Particle Size:

By following the next steps, the size of gold nanoparticles was measured by taking the average of 50 particles for each solution:

1. Measure micron bar with ruler.
2. If 1 μm = 2 mm on the ruler, then 1 mm on the ruler = 0.5 μm's.
3. Measure the diameter, or width of the particle with the ruler.
4. So, if a particle was measured by the ruler, and the width of it is 1 mm. Therefore, it's diameter is 0.5 microns.

3.1.2. Optical Spectroscopy

The energy related with electromagnetic radiation is defined by: $E = h\nu$; where E is energy (expressed in joules), h is Planck's const. (6.62×10^{-34} J-s), and ν is frequency of the radiation expressed in seconds [37]. Electromagnetic radiation can be viewed as electric and magnetic fields that travel through space in the form of a wave. Since radiation acts as a wave, it can defined either by its wavelength or frequency, which are related by: $\nu = c/\lambda$; where ν is the frequency expressed in seconds, c is the velocity of light (3×10^{8} ms^{-1}), and λ is wavelength of the radiation in meters. In UV-Vis spectroscopy, the wavelength is ordinarily communicated in units of nanometers (1 nm = 10^{-9} m) [37].

3.1.2.1. Electromagnetic Energy

At the point when radiation impinges on material, various interactions can take place, including reflection, transmittance, or absorbance. When measuring UV-Vis spectra, one measures the absorbance. Since light is a form of electromagnetic radiation that possesses some amount of energy, when it is absorbed by a material, it causes the energy of the atoms of molecules of the material to also increase through a form of energy transfer [36]. The

aggregate potential energy of a molecule, by and large, is defined by the sum of its electronic (E_e), vibrational (E_v), and rotational (E_r) energies: $E_t = E_e + E_v + E_r$; where E_t is the total energy. The measure of energy molecules possess in each configuration is not a continuum but rather a progression of discrete levels or states. The contrasts in energy among the distinctive levels are in the order: $E_e > E_v > E_r$ [45].

3.1.2.2. The basics of UV-visible spectroscopy

In some atoms, photons of UV and visible light have sufficient energy to excite electrons from one energy level to a higher energy levels [27]. However, for different molecules, vibrational and rotational energy levels are superimposed on the electronic energy levels and also interact with the incident radiation in several possible ways. At the point when light goes through or is reflected by the material, the measure of light absorbed is the difference between the intensity of the incident radiation (I_o) and the radiation transmitted by the sample (I). These are important parameters in UV-Visible spectroscopy that help determine sample concentration, such as particle size, bandgap, etc. The measure of light absorbed is communicated as either transmittance or absorbance. For most applications, absorbance values are utilized since the relationship between absorbance and concentration is a function of path-length which is the distance travelled by the light through the sample. UV-visible spectroscopy is typically utilized when studying liquids. This mode is less difficult and permits more precise quantitative investigation than do reflectance estimations on powder samples [27].

In our experiment, we used UV-vis spectrum to investigate the relationship between gold nanoparticles' sizes with peak positions and full width at half maximum (FWHM). Each

solution was carried on a 1 cm quartz cuvette before we insert it in the UV-visible spectroscopy.

3.2. Using Gold Nanoparticle to Grow Nanosprings

Noble metal nanosprings are an interesting category of materials that have enhanced surface areas, making them extremely useful in catalysis, flat panel displays, and nanoelectronics applications [41,20,25]. They are even utilized as extremely effective pressure sensors [18]. One of the simplest ways to synthesize nanosprings is through the introduction of a metal catalyst on the surface of the substrate, which in this case is silica. The method implemented here is a vapor liquid solid mechanism, where a liquid droplet of a colloidal suspension of the metal is placed on the substrate [40]. Colloidal monodispersed Au NPs were dropping known concentrations of Au NPs on a well-polished Si substrate.

3.2.1. Mechanism of Nanospring Growth

In all instances of helical development such as carbon nanotubes or nanosprings, there must be an asymmetry in the growth [3]. In the synthesis of nanosprings designed from a nanowire, it is the presence of contact angle anisotropy (CAA) at the interface between the nanowire and the nanoparticle catalyst that presents the asymmetry [25]. For the multi-nanowire nanosprings, CAA can't be the instrument driving this asymmetry [41]. A different mechanism in multi-nanowire nanospring development considers that the nanowires connect indirectly to form a kind of agglomerate. This is how it is assumed that the system behind the asymmetry is an opposition between the nanowires shaping the multi-nanowire nanosprings. In light of the fact that the nanowires framing the nanospring develop autonomously, the cooperation between them must be formed through the catalyst, which is Au NPs in our study. The individual nanowires fight with each other for Si and O contained inside the catalyst,

because of this opposition, growth rates of the nanowires vary. This contrasts in growth rates between the nanowires of the nanospring results in a torque on the catalyst, which produces the helical shape [25]. The contest may not generally give a proper reasoning for the growth of multi-nanowire nanosprings [41]. In short, as of now there is no authoritative clarification with reference to why different nanowires shape from a one kind of catalyst alone.

3.2.2. Growth Characterization Model:

The most recent growth characterization model for silicon nanosprings is by VLS that lead to the catalyst formation [43]. This growth characterization leads to the formation of asymmetric shaped Au-Si catalyst droplets that promotes the formation of amorphous nanowires. There will be no growth of silicon nanosprings with the absence of oxygen. The substrate will be heated to 250 °C while continuously flowing nitrogen. The nitrogen is used to carry the NS over the substrate. An addition of Silicon and oxygen will be done on the catalysts for 150s. Au-Si catalyst tips for a single nanospring will emerge from the edge of the bulk Au-Si catalyst. The second phase during the growth characterization is the formation of individual nanowires beneath the Au-Si catalyst, and it will be followed by a formation of Au-Si catalysts necking. The growth rates of individual nanosprings are directly related to their diameter [43].

3.2.3. Adjusting Settings of the Flow Controller

The flow controller parameters were adjusted in this experiment depending upon the growth time. Different nanoparticle growth times resulted in different sizes and depending on these sizes, the O_2 delay start and stop, precursor, reactor, and injector flow rated were all adjusted. For example, for a nanoparticle growth time of 120 min, the O_2 delay start and stop flow rates were set at 20 sec. For the same growth time, the IR heater, the reactor, precursor

and injector flow rates were set at 460, 270, 50, and 199 sec. respectively. The flow controller also controls the precursor ramp rate for the pressure, the N_2 and the O_2 sccm flow rates as 5, 30, and 7.0 respectively.

3.2.4. Fabrication of nanosprings

The nanoparticles were grown on the Si substrate by gently warming the substrate in a controlled environment for about 2 hours. Si is used in the fabrication of nanosprings because of its ability to undergo strain and in the process form nanometer sized heteroepitaxial bilayers. Si wafers undergo anisotropic deformation along a particular direction which is what results in its helical or spring like structure [3]. On this substrate, measured amounts of gold nanoparticles solutions were dropped and allowed to dry. After drying, the sample was remeasured and then put it in a growing system (a vapor liquid solid) for two hours. After that time, the growing system cooled down, the chamber was opened to take out the sample, and measure it for the third time to obtain a nanosprings' mass. Following this, SEM images were collected to measure the length of the nanosprings.

CHAPTER 4: Results

4.1. Colloidal Gold Solutions:

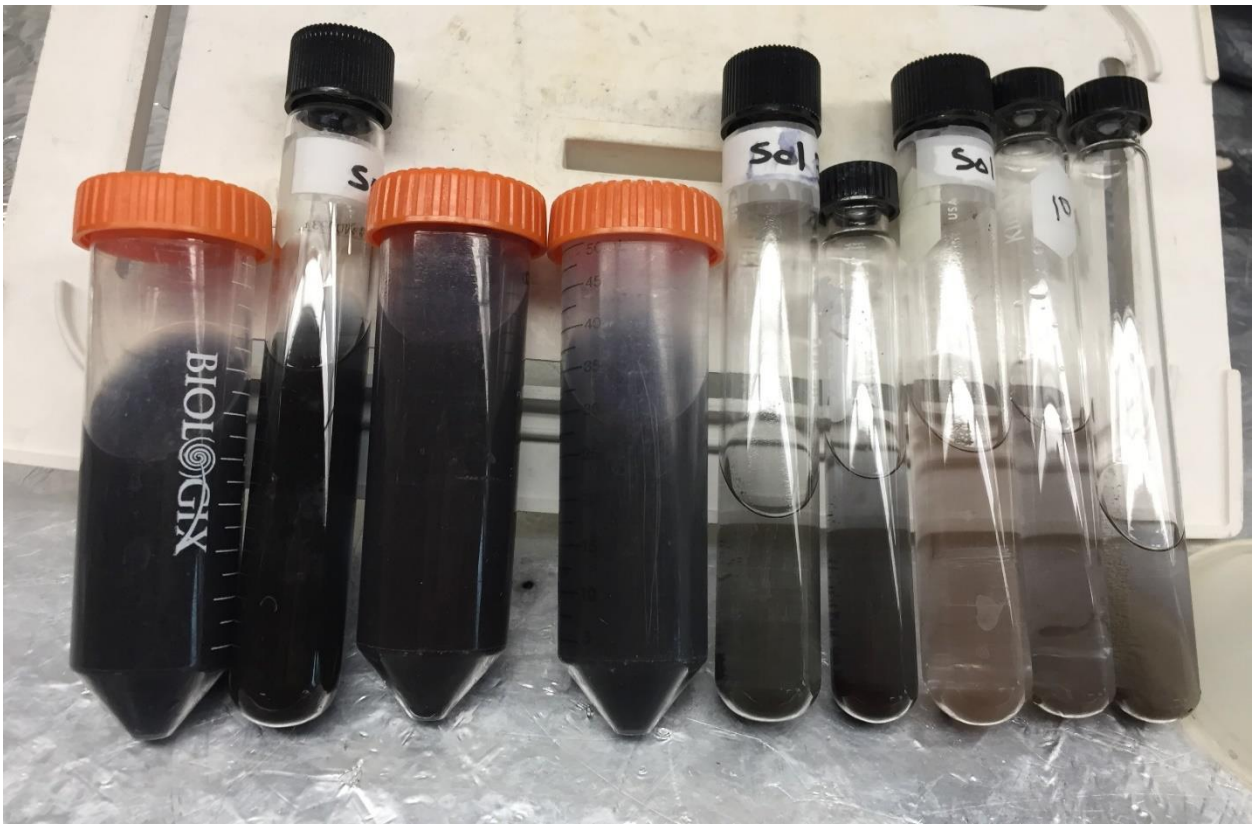

Figure 4.1: Various colors of gold nanoparticle solutions indicate different sizes of Au NPs.

As it can be seen in the previous picture, the various concentrations of $AuCl_3$ and trisodium citrate resulted in different colored solutions. Those solutions contain a fluid that has colloidal suspension of nanoparticles of gold, which are referred to as colloidal gold. The variety of colors of colloidal gold depends on the particles' diameter. For the first tube from the left, when the color is deep black, the solution has the biggest particles. However, the solutions get lighter when we move to the right side until the last one, which has the smallest particles.

4.2. Scanning Electron Microscopy:

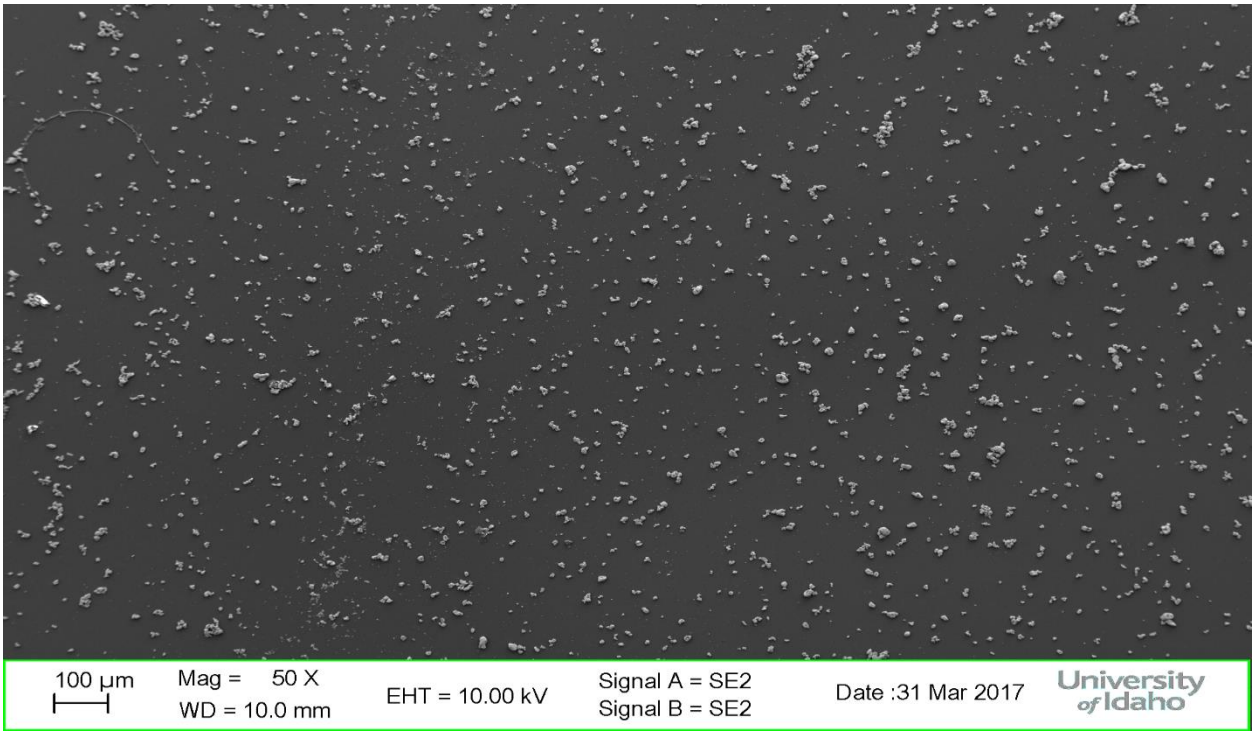

Figure 4.2: SEM Image of Gold Nanoparticles with 5 mg Au concentration

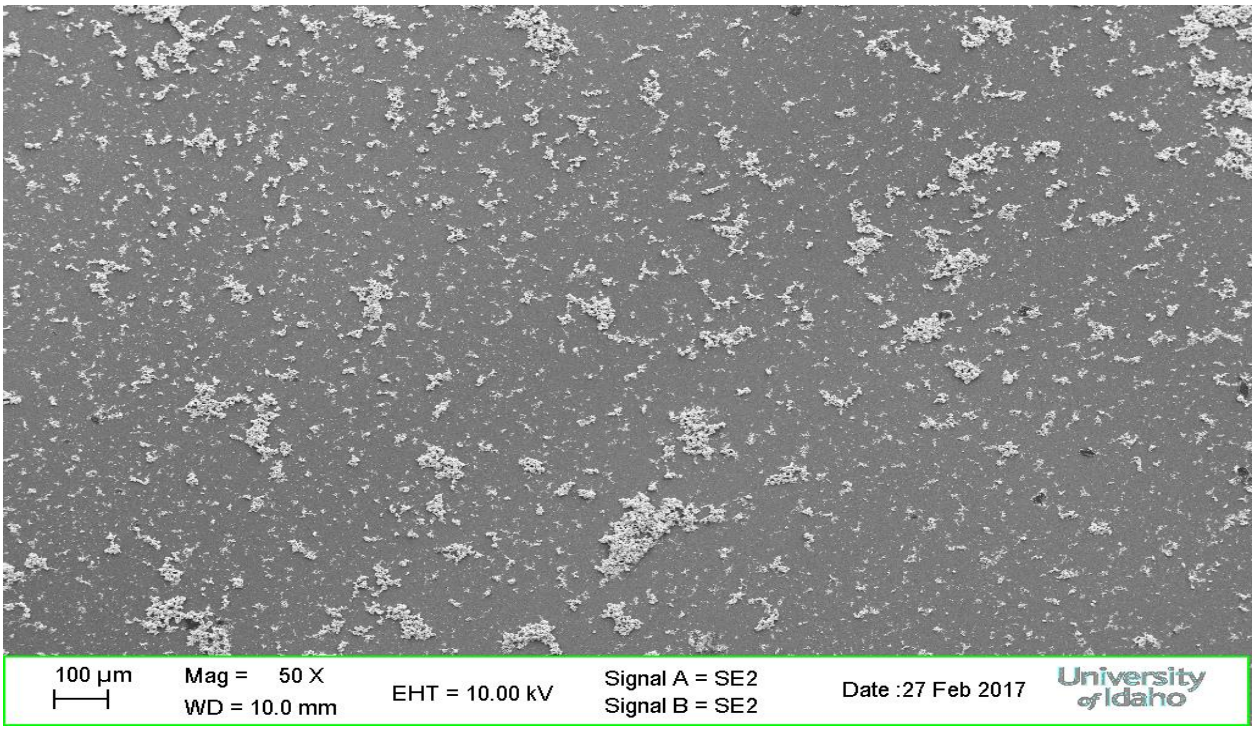

Figure 4.3: SEM Image of Gold Nanoparticles with 10 mg Au concentration

Shown in Figure 4.2 and 4.3 are typical SEM images of gold nanoparticles viewed at 50x magnification with Au concentrations of 5 and 10 mg respectively. These particles have nearly spherical shapes. As presented in figure 4.2, we can clearly see that the SEM image shows less Au nanoparticles and more uniform shapes compared to figure 4.3.

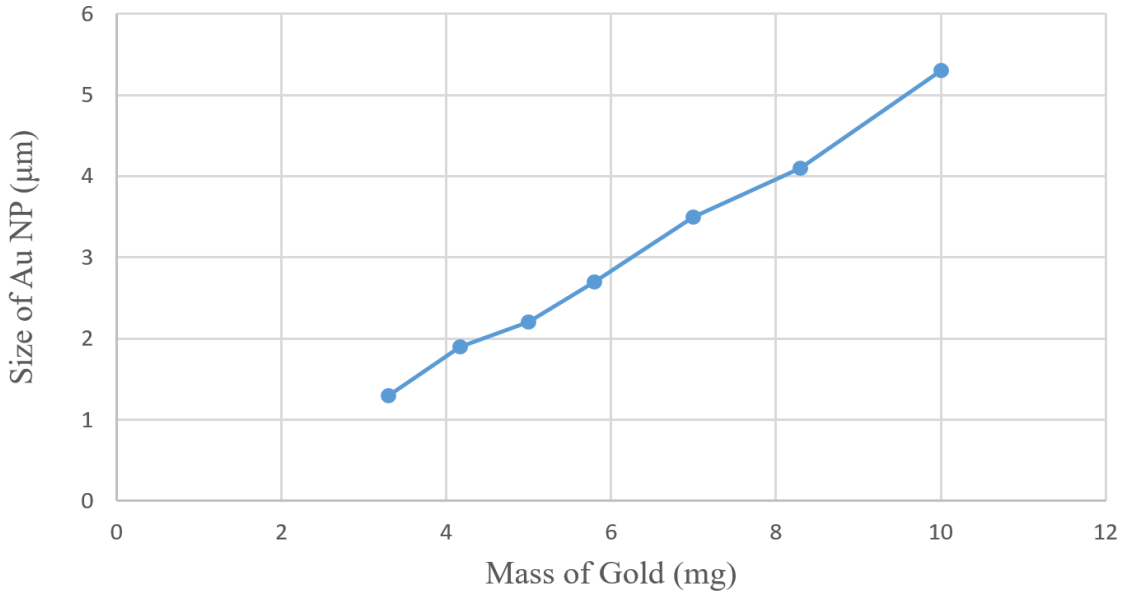

Figure 4.4: The size of the gold nanoparticles when the concentrations of $AuCl_3$ and trisodium citrate are increased.

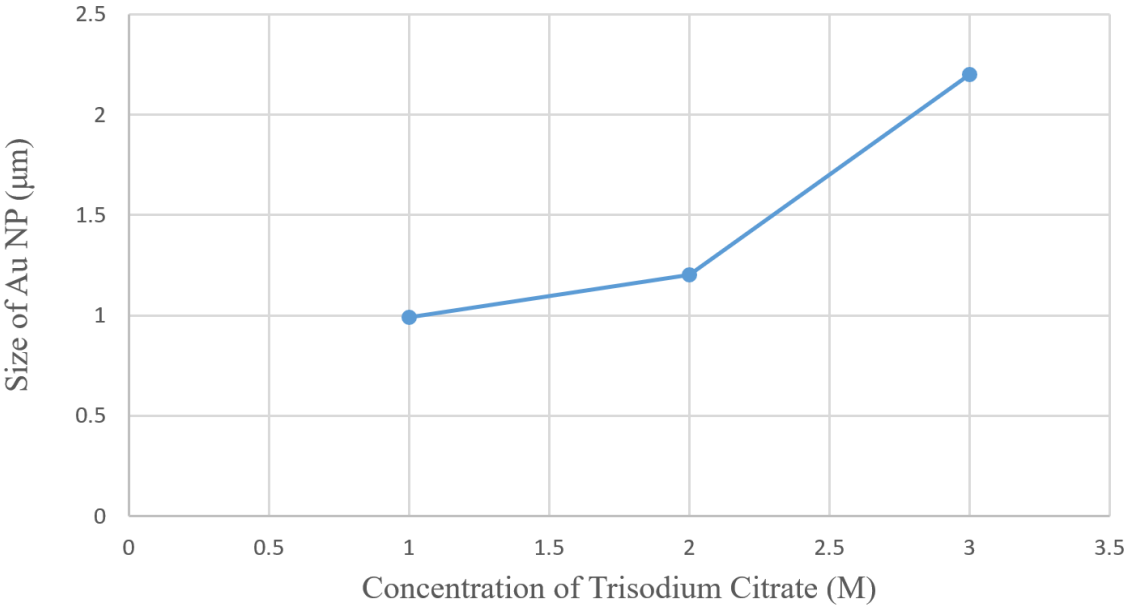

Figure 4.5: The size of gold nanoparticles when the concentration of trisodium citrate is decreased with keeping the same amount of $AuCl_3$.

The different concentrations of $AuCl_3$ and trisodium citrate resulted in different sizes of Au NPs with average diameters between 0.99 and 5.3 µm as it can be observed in figures

4.4 and 4.5. Form solution 1 until 7, when the concentrations of $AuCl_3$ are increased gradually with the concentrations of trisodium citrate, the size of the existing particles is steadily increased as well as the size distribution. However, the same amount of $AuCl_3$ was kept with reducing the trisodium citrate progressively for solutions 8 and 9 which resulted in reducing the gold nanoparticles' size.

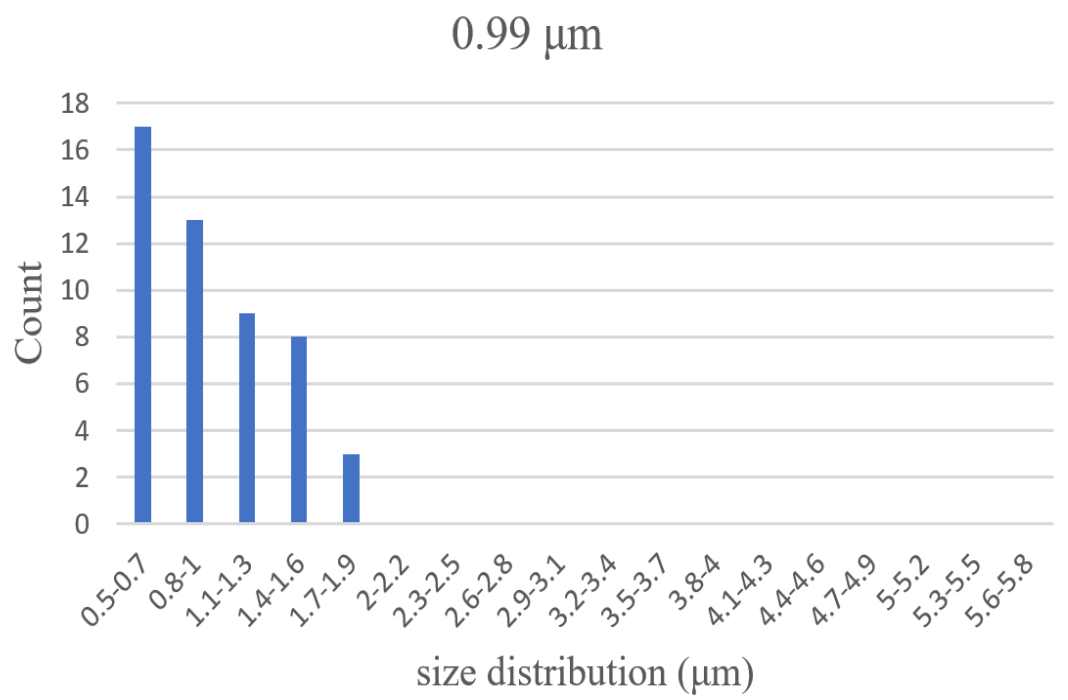
0.99 µm
Count
18
16
14
12
10
8
6
4
2
0
0.5-0.7
0.8-1
1.1-1.3
1.4-1.6
1.7-1.9
2-2.2
2.3-2.5
2.6-2.8
2.9-3.1
3.2-3.4
3.5-3.7
3.8-4
4.1-4.3
4.4-4.6
4.7-4.9
5-5.2
5.3-5.5
5.6-5.8
size distribution (µm)

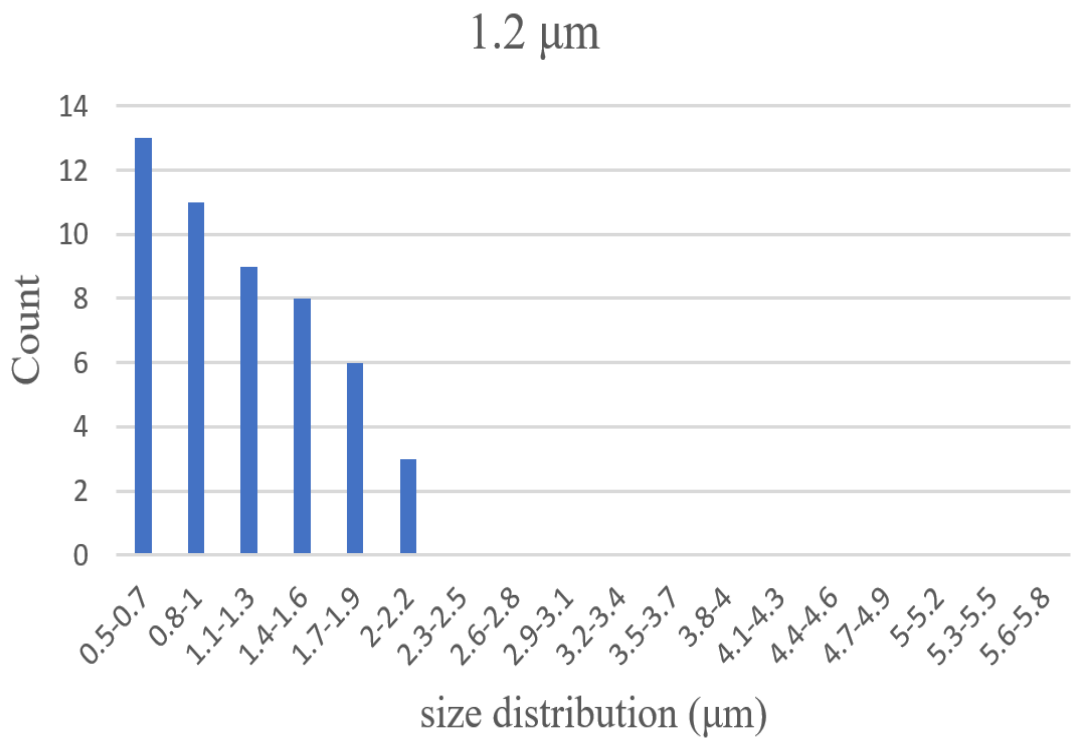
1.2 µm
Count
14
12
10
8
6
4
2
0
0.5-0.7
0.8-1
1.1-1.3
1.4-1.6
1.7-1.9
2-2.2
2.3-2.5
2.6-2.8
2.9-3.1
3.2-3.4
3.5-3.7
3.8-4
4.1-4.3
4.4-4.6
4.7-4.9
5-5.2
5.3-5.5
5.6-5.8
size distribution (µm)

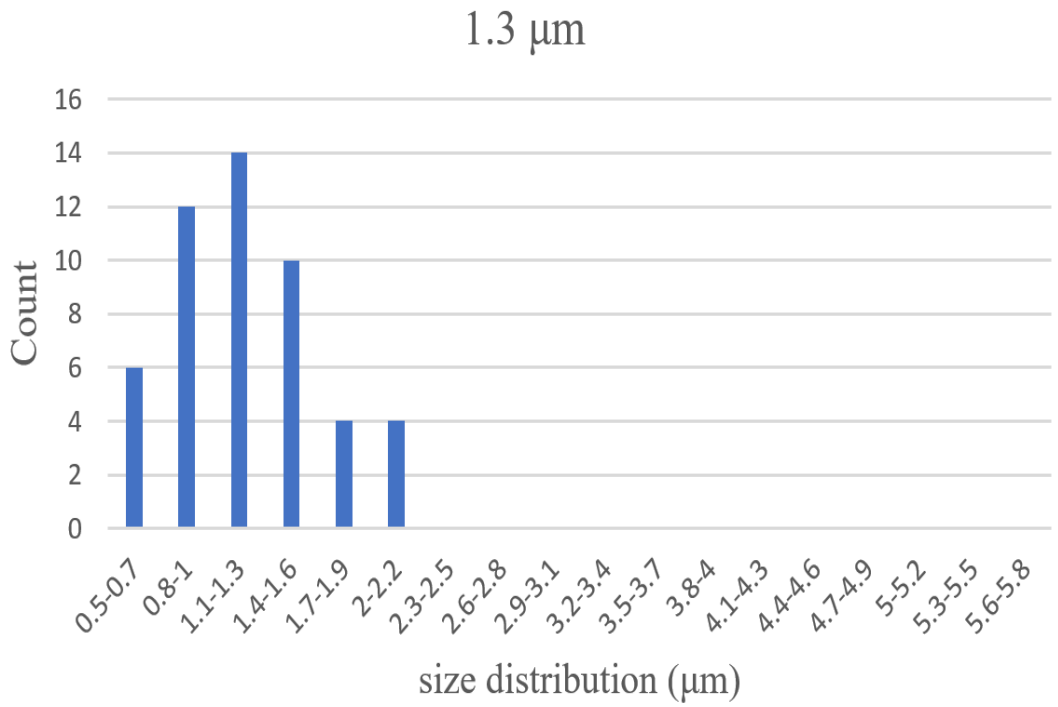
1.3 µm
Count
16
14
12
10
8
6
4
2
0
0.5-0.7
0.8-1
1.1-1.3
1.4-1.6
1.7-1.9
2-2.2
2.3-2.5
2.6-2.8
2.9-3.1
3.2-3.4
3.5-3.7
3.8-4
4.1-4.3
4.4-4.6
4.7-4.9
5-5.2
5.3-5.5
5.6-5.8
size distribution (µm)

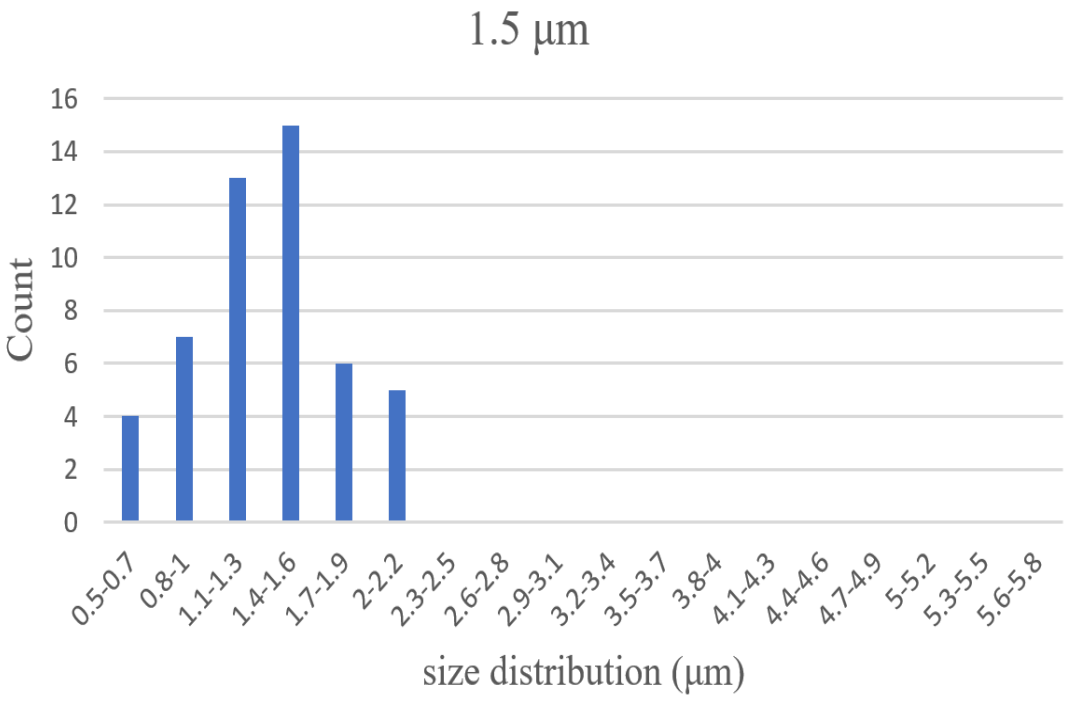
1.5 µm
Count
16
14
12
10
8
6
4
2
0
0.5-0.7
0.8-1
1.1-1.3
1.4-1.6
1.7-1.9
2-2.2
2.3-2.5
2.6-2.8
2.9-3.1
3.2-3.4
3.5-3.7
3.8-4
4.1-4.3
4.4-4.6
4.7-4.9
5-5.2
5.3-5.5
5.6-5.8
size distribution (µm)

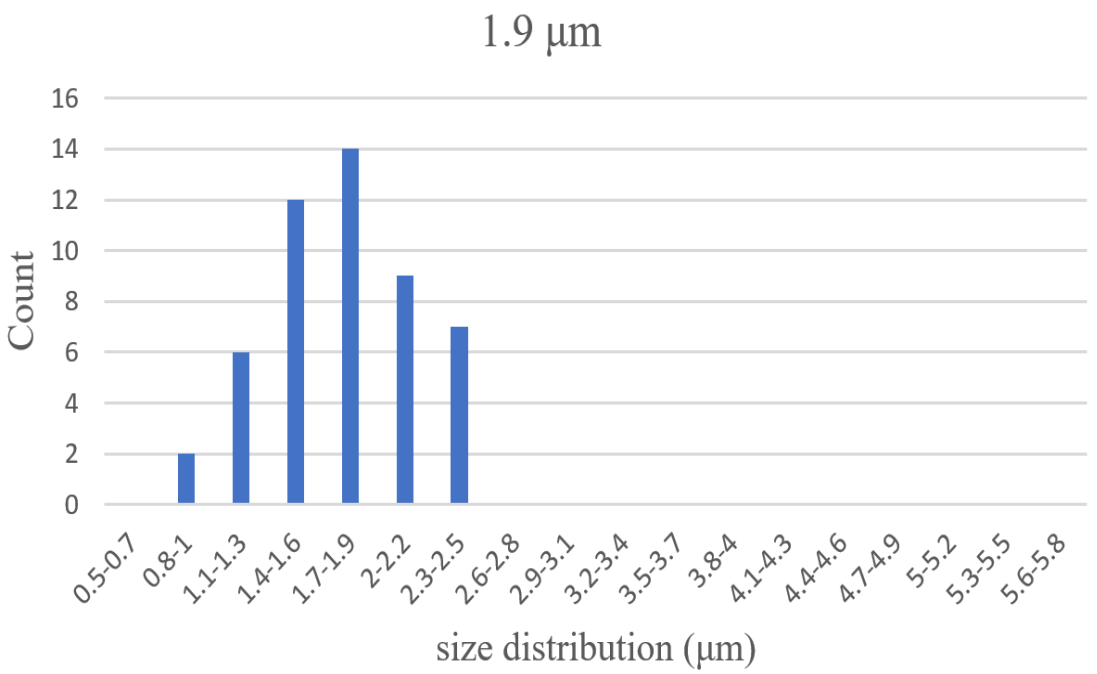
1.9 µm
Count
16
14
12
10
8
6
4
2
0
0.5-0.7
0.8-1
1.1-1.3
1.4-1.6
1.7-1.9
2-2.2
2.3-2.5
2.6-2.8
2.9-3.1
3.2-3.4
3.5-3.7
3.8-4
4.1-4.3
4.4-4.6
4.7-4.9
5-5.2
5.3-5.5
5.6-5.8
size distribution (µm)

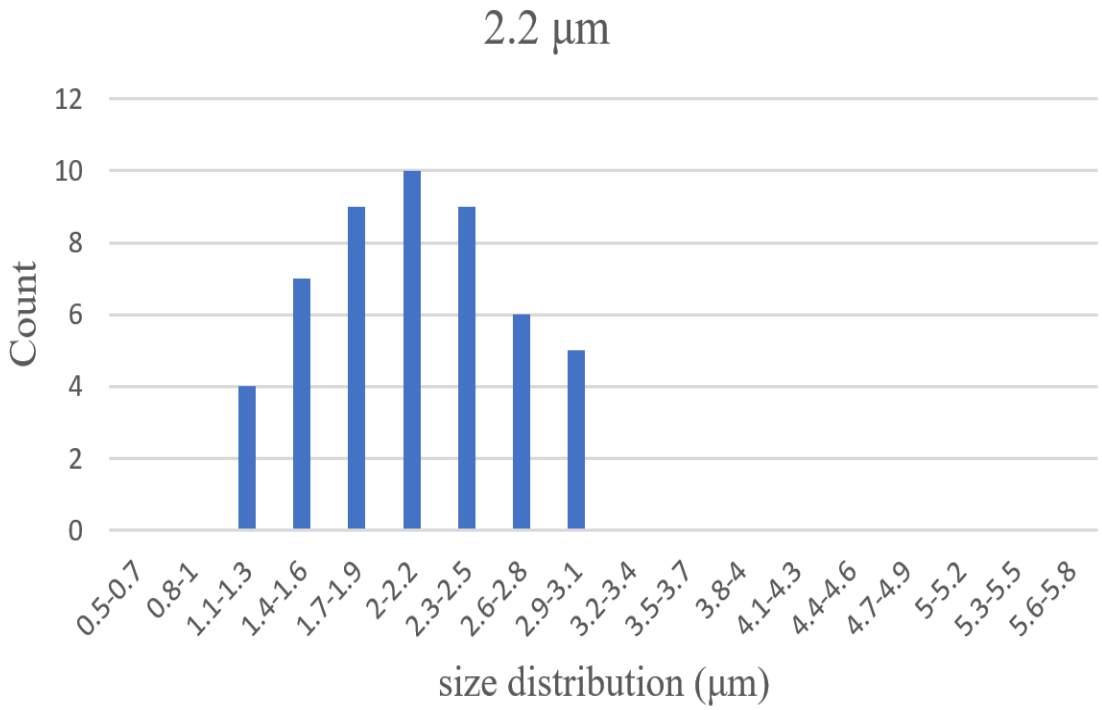
2.2 µm
Count
12
10
8
6
4
2
0
0.5-0.7
0.8-1
1.1-1.3
1.4-1.6
1.7-1.9
2-2.2
2.3-2.5
2.6-2.8
2.9-3.1
3.2-3.4
3.5-3.7
3.8-4
4.1-4.3
4.4-4.6
4.7-4.9
5-5.2
5.3-5.5
5.6-5.8
size distribution (µm)

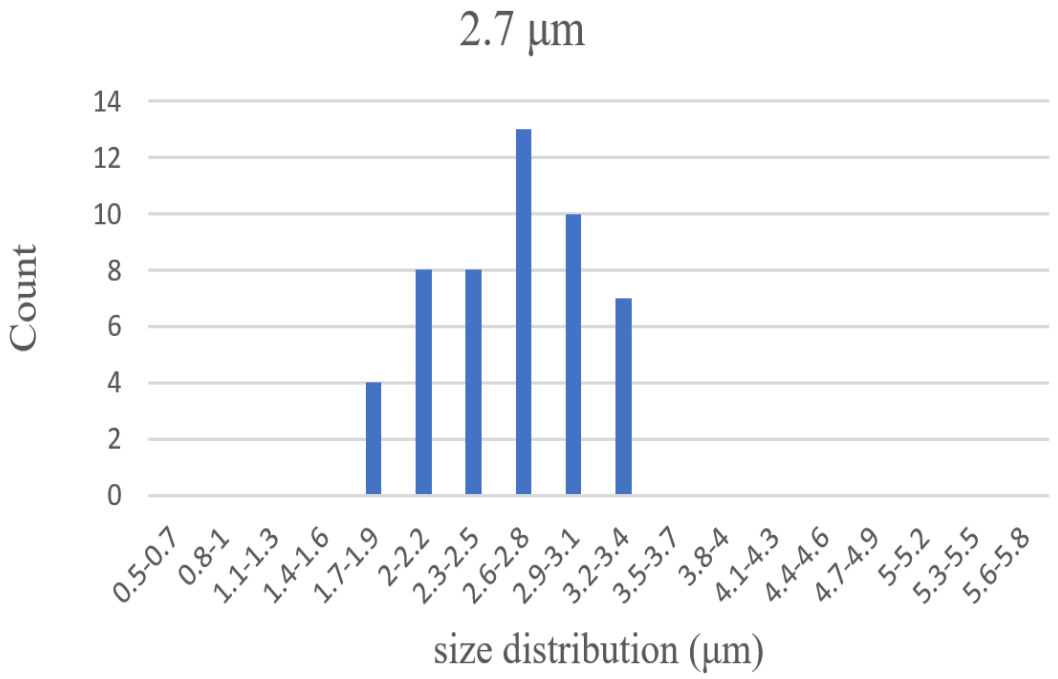
2.7 µm
Count
14
12
10
8
6
4
2
0
0.5-0.7
0.8-1
1.1-1.3
1.4-1.6
1.7-1.9
2-2.2
2.3-2.5
2.6-2.8
2.9-3.1
3.2-3.4
3.5-3.7
3.8-4
4.1-4.3
4.4-4.6
4.7-4.9
5-5.2
5.3-5.5
5.6-5.8
size distribution (µm)

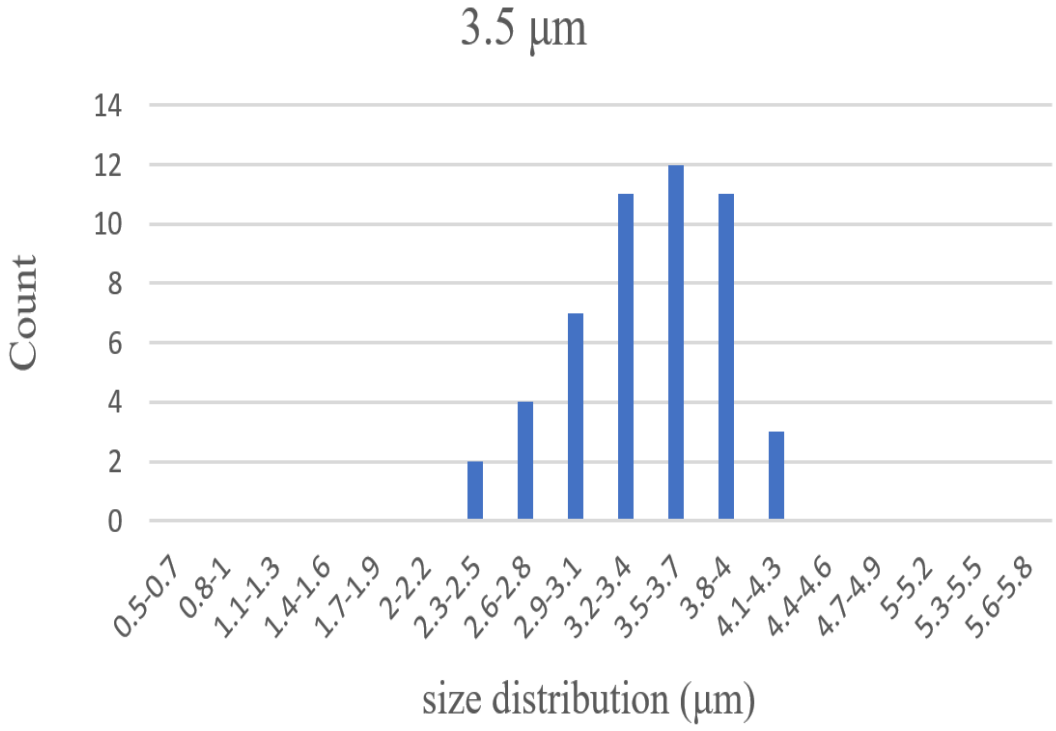
3.5 µm
Count
14
12
10
8
6
4
2
0
0.5-0.7
0.8-1
1.1-1.3
1.4-1.6
1.7-1.9
2-2.2
2.3-2.5
2.6-2.8
2.9-3.1
3.2-3.4
3.5-3.7
3.8-4
4.1-4.3
4.4-4.6
4.7-4.9
5-5.2
5.3-5.5
5.6-5.8
size distribution (µm)

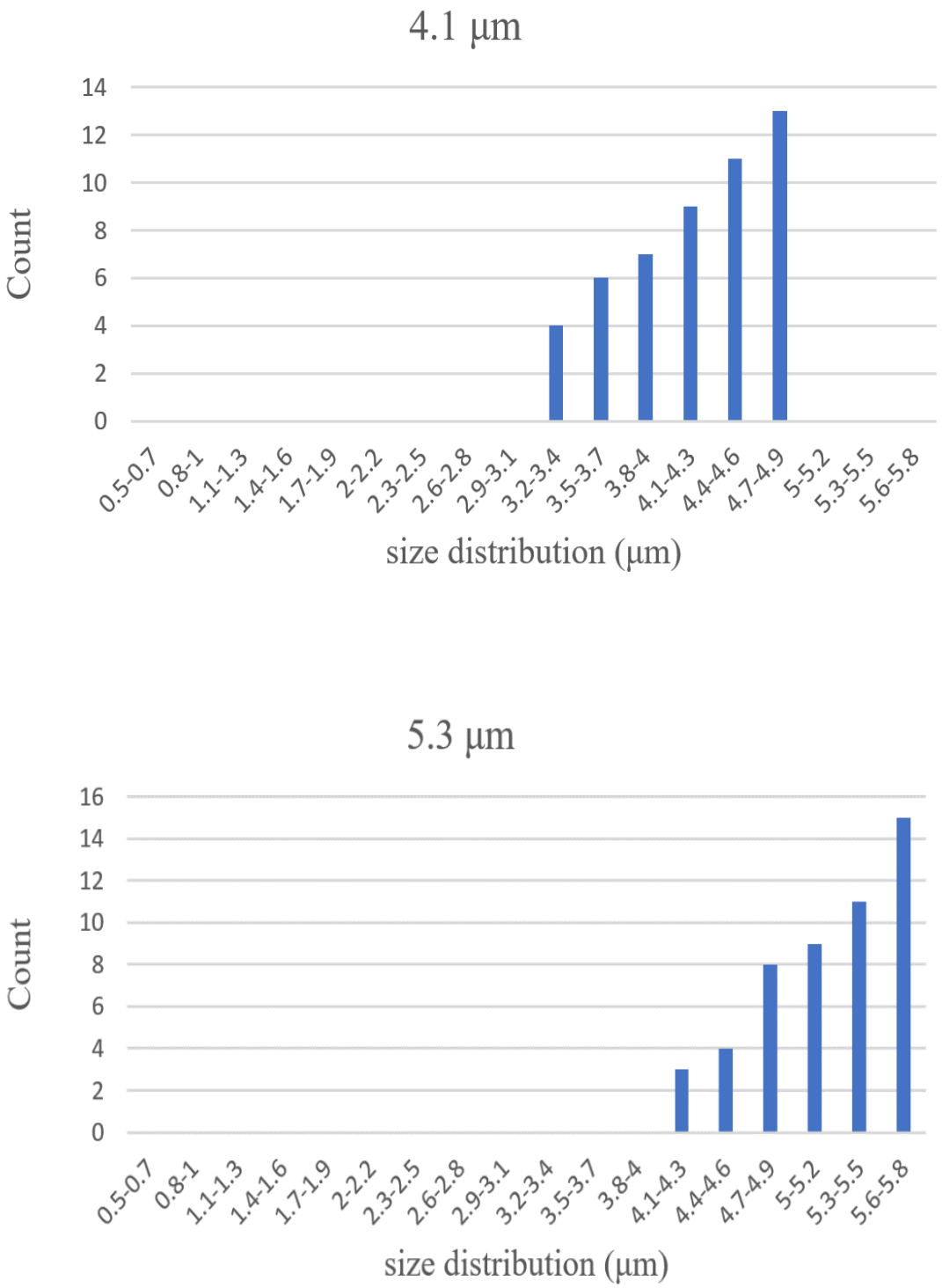

Figure 4.6: The size distributions of different sizes of gold nanoparticles

Figure 4.6 illustrates the size distribution of various sizes of gold nanoparticles. In all cases the range of particle sizes is about 2 microns. Interestingly, the shape of the distribution changes systematically with the mean particle size. When the size of the particle is small, the curve is skewed left. However, the curve is skewed right when the size of the particle is big. The latter might be because larger particles are obscured by aggregates.

4.3. The UV-Visible Spectroscopy:

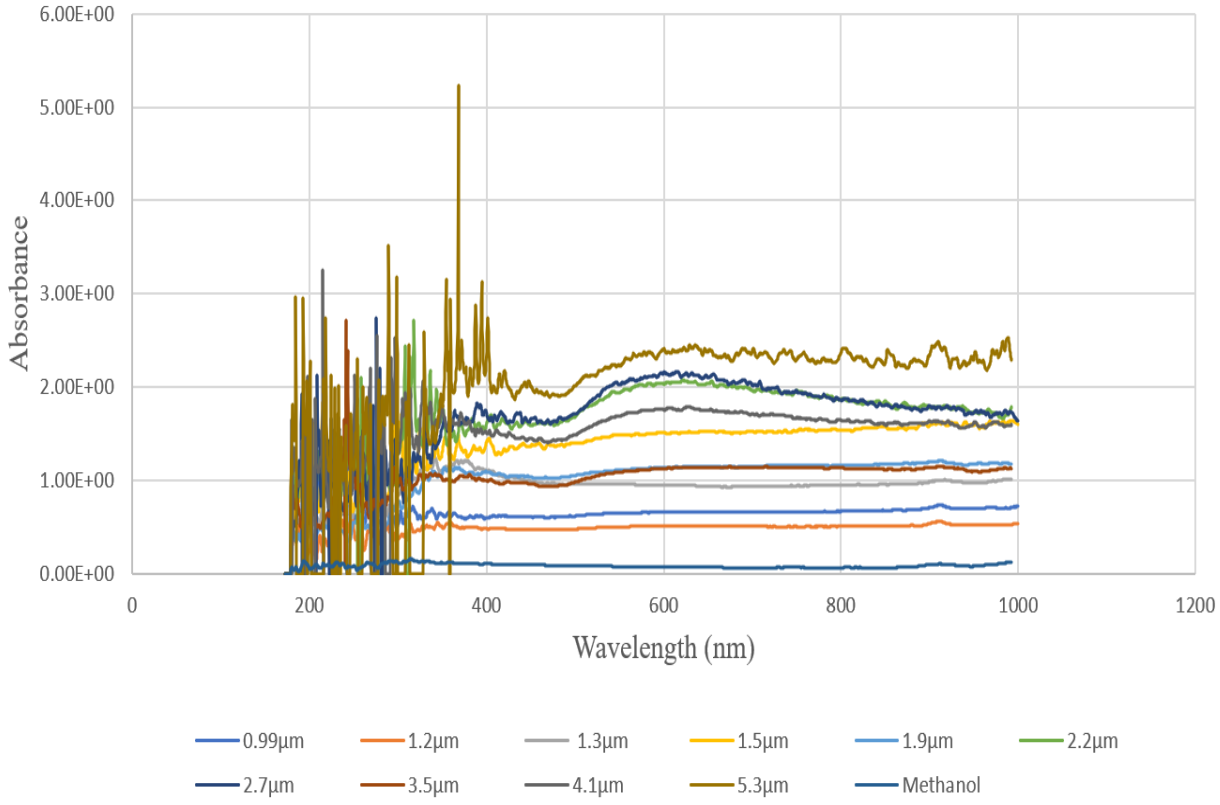

Figure 4.7: The effect of spherical gold nanoparticles with various diameters on the surface plasmon absorption. The UV-vis absorption spectra of colloidal gold solutions of nanoparticles with diameters changing between 0.99 and 5.3 µm present that the absorption maximum red-shifts with increasing particle diameters.

Figure 4.7 displays the UV-visible spectrum of the different sizes of gold nanoparticles with diameters of 0.99, 1.2, 1.3, 1.5, 1.9, 2.2, 2.7, 3.5, 4.1, and 5.3 µm. As we can see, clear absorption peaks can be observed for all Au NPs except for 1.3 µm, which hold wavelength at the range of 572 – 674.5 nm.

In this study, when we plotted absorbance verses wavelength for each solution individually, there was a broad peak around 500-600 nm. We estimate this peak's position and

width using the following procedure. First we identify the points on the curve with the maximum and minimum absorbance. We then find the two points on the curve which have an absorbance exactly half-way between these two values. The wavelength difference between these two points provides our estimate of the FWHM. By the same way, we determined the peak position, which is the point of maximum absorbance. However, for all the curves except for 1.2 μm, the right edge did not show sufficient decrease to determine the peak's width, so we applied the same method in the left side which fit clearly, and then multiplied it by two to have FWHM.

Particle Size (μm)	Peak Position (nm)	FWHM (nm)
0.99	572	52
1.2	587	109
1.3	Can't be observed	Can't be observed
1.5	590	112
1.9	601	152
2.2	613	171
2.7	635	206
3.5	630	227
4.1	650	247
5.3	674.5	262

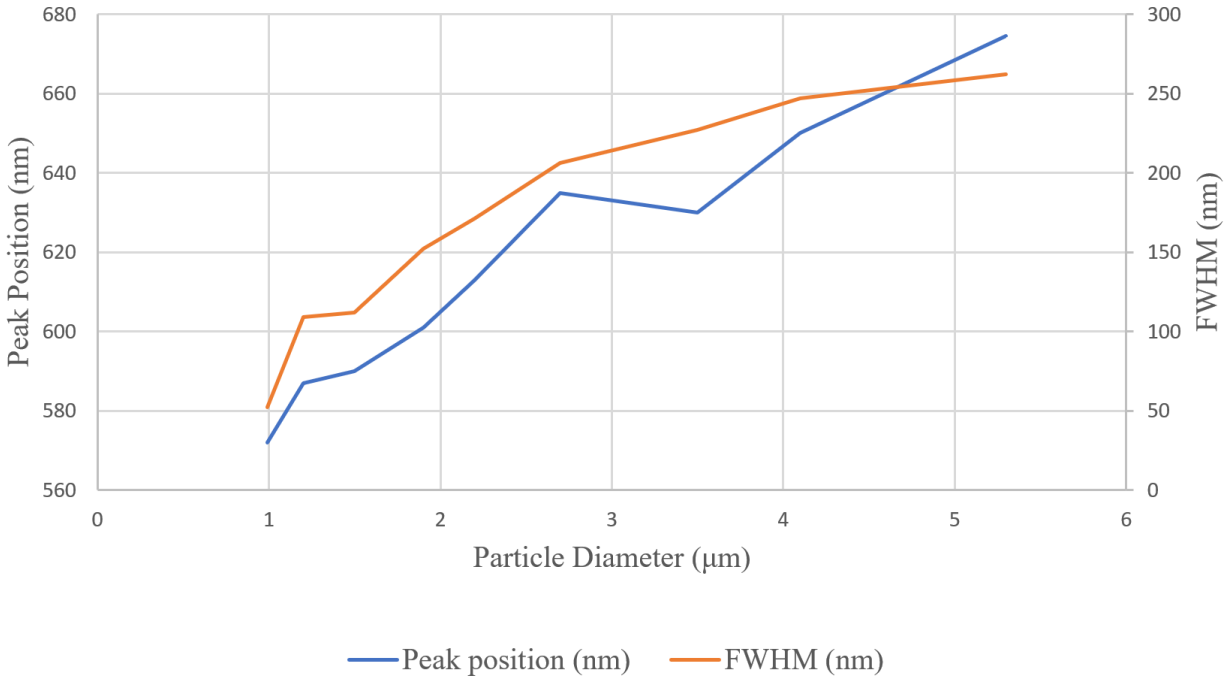

Figure 4.8: The relationship between the particle diameter with the corresponding peak position in the left side and the corresponding FWHM in the right side

The relationship between the particles' diameter with the corresponding peaks' position and the full width at half maximum (FWHM) is illustrated in figure 4.8. It is visible that the peak position shifts to longer wavelength with increasing the particle size as well as FWHM.

4.4. Silica Nanosprings:

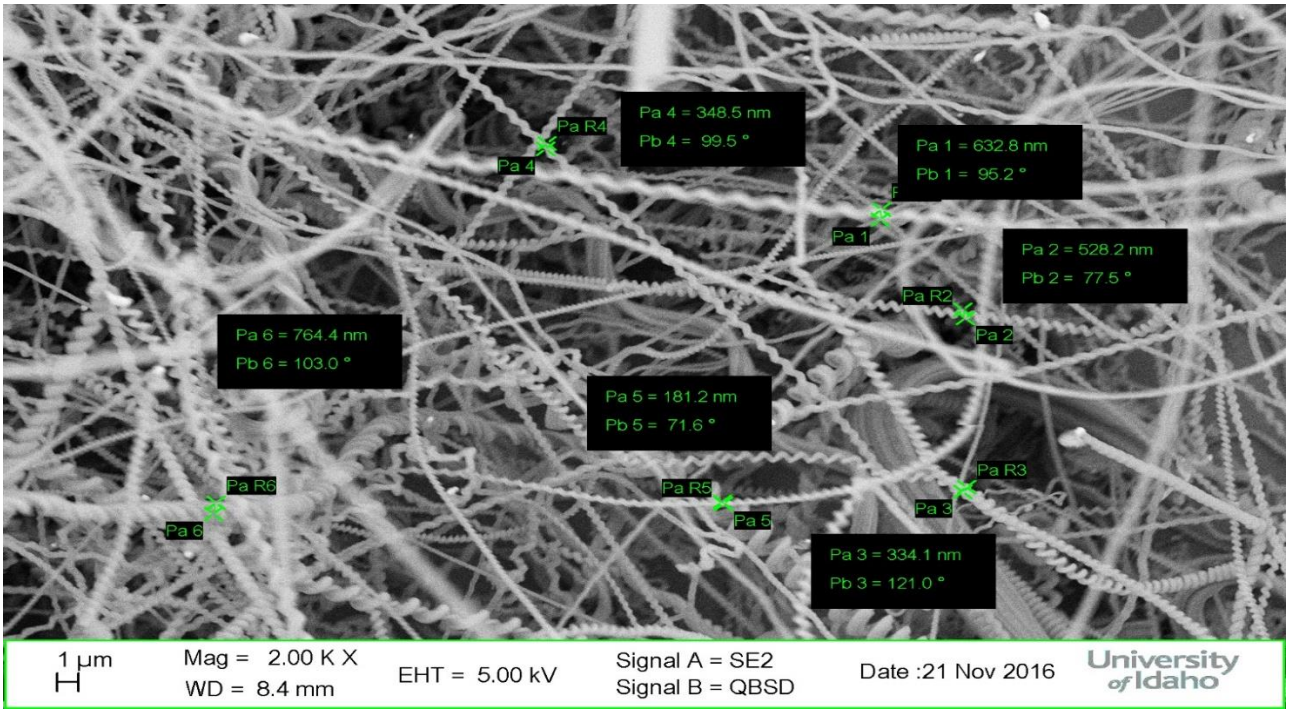

Figure 4.9: The best width of Si nanosprings coated with Au NPs

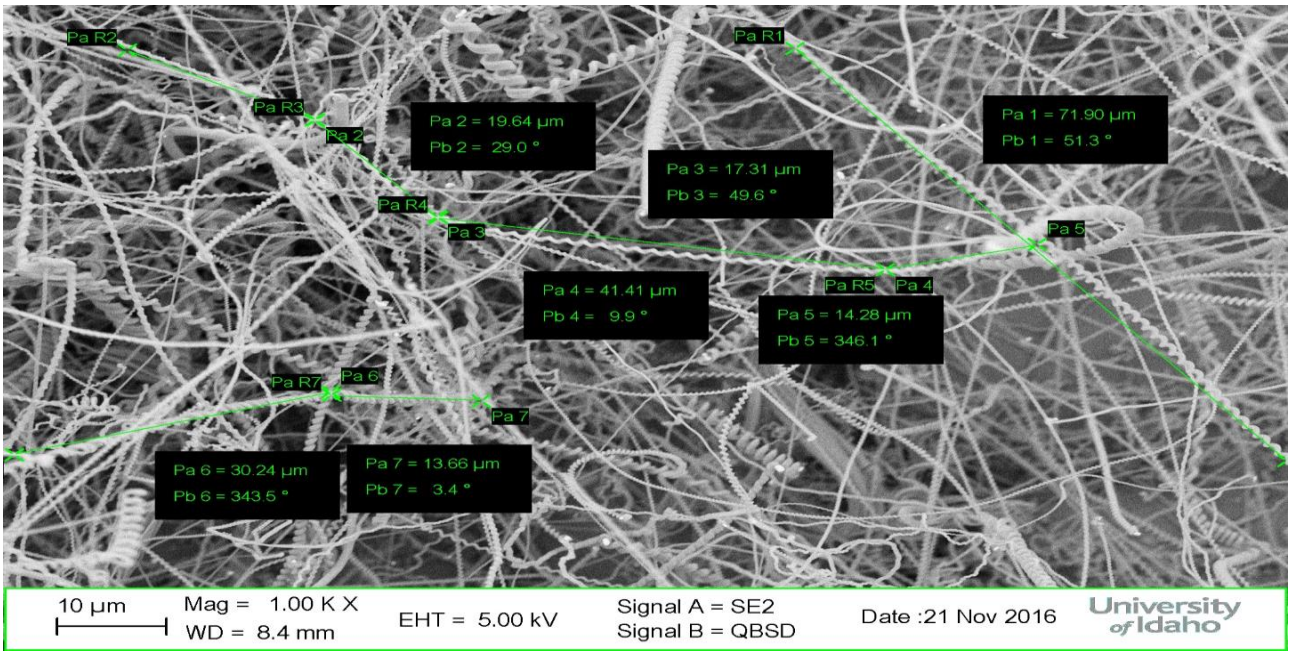

Figure 4.10: The best lengths of Si nanosprings coated with Au NPs

Scanning electron microscopy helped to determine different sizes of Si nanosprings obtained by different sizes of gold nanoparticles. In this work, we investigated the Si nanosprings obtained by vapor liquid solid growth mechanism, and we found a heterogeneous distribution of sizes. Figures 4.9 and 4.10 present the SEM images for the best width and length of Si nanosprings. The best widths vary from 181 nm to 764 nm while the best lengths range from 13 μm to 72 μm. These show the best Si nanosprings with Au nanoparticle's size 2.2 μm compared to other sizes.

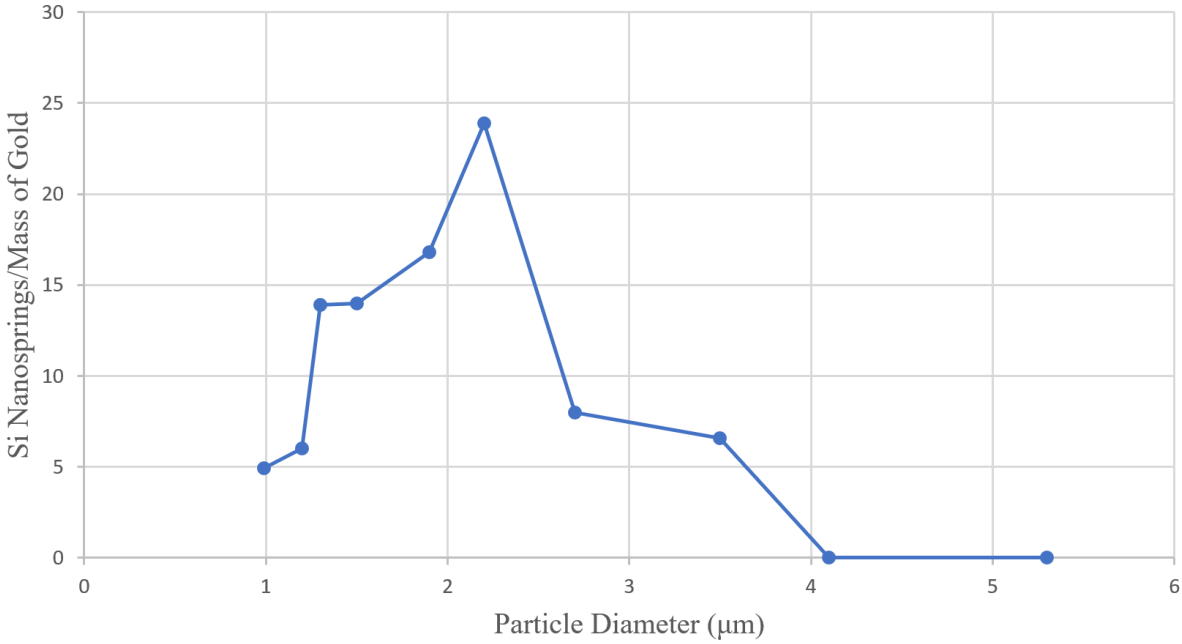

Figure 4.11: The Relationship Between the Ratio of Si nanosprings to Mass of Gold Nanoparticles with the Size of Gold Nanoparticles

The previous figure examined the ratio of Si nanosprings' mass to the mass of Au NPs compared against the size of colloidal gold nanoparticles and it was seen that there is a threshold limit for the size of the colloidal gold nanoparticles beyond which the mass of both Si nanosprings to Au NPs ratio decrease. In this study, the ratio of mass of nanosprings to the mass of Au NPs increased for Au NP sizes between 1µm to about 2.2µm, beyond which the ratio decreased until it disappeared as we can see in figure 4.11.

CHAPTER 5: Discussion

5.1. Colloidal Gold Solutions:

In this work, we don't really see distinct colors because we have a broader distribution of particles, as compared to what "Gold Nanoparticles: Properties and Applications" state [14]. They declare that for small gold nanoparticles nearly about 30nm, the light absorbance will be in the blue-green portion of the spectrum while red light will be reflected, which is caused by the surface plasmon resonance phenomenon. That resulted in a bright red color. However, as the particle size get bigger, the red light will be absorbed while the blue light will be reflected due to the same phenomenon, which produces solutions with a pale blue or purple color [14]. The reason is that this study wasn't focused on making very narrow size distributed solution of gold colloids, but exploring the range of sizes that most efficiently produces nanosprings.

5.2. Scanning Electron Microscopy:

In this experiment, the size and shape of Au NPs were investigated. From the SEM data shown in figures 4.4 and 4.5, they are evident that the size of Au NPs depends on the concentrations of both $AuCl_3$ and trisodium citrate. Those figures demonstrate the Au NPs average diameters between 0.99 and 5.3 μm. For the first seven solutions, when the concentrations of both $AuCl_3$ and trisodium citrate are increased, the size of gold nanoparticles is increased as well as the gold nanoparticles' size distribution. Therefore, a direct relationship between the concentration of $AuCl_3$, trisodium citrate, and size of the Au NPs can be seen from the results. However, when we attempted to minimize the gold nanoparticles' size, we kept the same amount of $AuCl_3$ with reducing the trisodium citrate progressively for the last two solutions.

5.3. The UV-visible spectroscopy:

Displayed in Figure 4.7 is the absorbance spectra of Au NPs with diameter of 0.99-5.3 μm, which is characterized by absorption bands in the range of 572 – 674.5nm with surrounding medium refractive index 1.33, which is methanol in our experiment. According to Seney et al. these bands are ascribed to transverse surface plasmon resonances (SPR) [32]. The peak intensity of this band (peak position) shifts in wavelength as a function of the diameter of the Au nanoparticle. Theory predicts that Au SPR peak is size dependent and red-shifts with an increase in size of the nanoparticles [32,6,29]. This theory is confirming what we investigated in figure 4.8 where the different sizes of Au NPs controlled the SPR absorption band since we have the same surrounding medium refractive index. Thus, as expected, a linear relationship between particle diameter and wavelength can be seen from the peak position and FWHM verses size plot as it can be seen in figure 4.8.

From the presented data, we can see that the position of the peak and FWHM depend on the size of gold nanoparticles. As the size of the nanoparticles increases also the peak position shifts to longer wavelength and peak broadening (increasing FWHM). This proves the theory of the same which states that the increase of the particle size also directly increases the FWHM, which can be explained using the optical processes. While the size of a nanoparticle is smaller than the wavelength, then only the absorbance can occur at this point. Thus, when there is an increase of a particle size, then scattering also becomes dominant hence the peak becomes broader and broader [15].

When electromagnetic waves inflow through a matter, the wastage of energy results from absorption and scattering. The absorbance of light occurs when the energy of photon is dissipated because of inelastic operations. However, the scattering of light results when the

energy of photon causes electron oscillation in the material that emits photons in the shape of scattered light at a shifted frequency or at the same incident light's frequency [9].

By comparing our data with reported work, it can be seen that they studied the relationship between the size of gold nanoparticles and peak positions and line width, and they investigated that the size of gold nanoparticles is directly proportional to line width and peak position, i.e. as the size of nanoparticles also increases the peak positions and line width increases [23]. Thus, we can clearly say that, their results are consistent with our results which indicates the size of nanoparticles is directly proportional to the line width and peak positions. From the results we have obtained in this experiment we can conclude that the increase in the size of Au nanoparticles influenced the increase of the position peaks and FWHM.

5.4. Silica Nanosprings:

In this study, Si nanosprings were fabricated on silica substrates that has Au NPs on top of it by using VLS growth. As what we indicated before, different concentrations of colloidal gold were obtained from different concentrations of both $AuCl_3$ and trisodium citrate. The more the concentration of $AuCl_3$ and trisodium citrate, the more was the quantity of Au NPs produced and larger was the particle size of Au NPs. Different concentrations of colloidal gold were used to fabricate springs of different sizes. The most well-formed Si nanosprings is with Au nanoparticle's size 2.2 μm. The widths are ranging from 181 nm to 764 nm and lengths are ranging between 13 μm to 72 μm were observed from the SEM images as it is shown in figure 4.9 and 4.10.

It has been reported in literature that different metal nanoparticles and different deposition techniques can produce nanosprings of different dimensions and properties [44, 47, 24, 2]. Since we used one technique to make Silica nanosprings, which depends on the VLS mechanism, those different dimensions and properties are probably due to the size

distributions of various colloidal gold droplets' diameters. In our experiment, as the size of the colloidal gold droplets increase, the Au NPs would have aggregated in the surface, which resulted in preventing the formation of Si nanosprings, compared with what Abdeddaïm et al., states, with increasing of sizes, the stability of the droplet of the same volume for a smaller size becomes difficult to maintain at larger nanoparticle sizes [1]. As what we found in our result, when the Au NPs became bigger, no ratio between mass of both Si nanosprings and gold were shown. Therefore, Si nanosprings are size dependent.

CHAPTER 6: Conclusion

Au NPs were synthesized through a well known citrate reduction method, described by Turkevic. In another method, decreasing concentrations of trisodium citrate was used to decrease the sizes of these Au NPs. These Au NPs were characterised by using SEM. The SEM images illustrated those Au NPs are spherical. The optical properties of colloidal Au NPs were studied through UV-visible absorption spectroscopy, and an absorption maximum as well as FWHM was observed for each solution, which was also characteristic of Au NPs. The linear change in absorption maxima and FWHM with the size of the NPs have also been described in detail. In addition, Colloidal Au NPs of different sizes were dropped on silicon substrates to fabricate high performance nanosprings. SEM images were analysed and there was clear relationship between the mass of nanosprings to the mass of gold ratio and the size of the Au NPs that was established. A critical Au NP size of about 2.2μm was identified as the critical size beyond which the size to mass ratio decreased. Thus, the formation of nanosprings depends on the size and size distribution of Au NPs.

References

1. Abdeddaïm, R. et al. "Negative Permittivity And Permeability Of Gold Square Nanospirals." *Applied Physics Letters* 94.8 (2009): 081907. Web. 1 Aug. 2017.
2. Bajaj, Rajeev. "Nanospring." U.S. Patent No. 7,759,165. 20 Jul. 2010.
3. Bell, D. J., et al. "Three-dimensional nanosprings for electromechanical sensors." *Sensors and Actuators A: Physical* 130 (2006): 54-61.
4. Brown, Sarah D. et al. "Gold Nanoparticles For The Improved Anticancer Drug Delivery Of The Active Component Of Oxaliplatin." *Journal of the American Chemical Society* 132.13 (2010): 4678-4684. Web. 28 July 2017.
5. Burda, Clemens et al. "Chemistry And Properties Of Nanocrystals Of Different Shapes." *Chemical Reviews* 105.4 (2005): 1025-1102. Web. 28 July 2017.
6. Chen, Wei-Ta, Ting-Ting Yang, and Yung-Jung Hsu. "Au-Cds Core−Shell Nanocrystals With Controllable Shell Thickness And Photoinduced Charge Separation Property." *Chemistry of Materials* 20.23 (2008): 7204-7206. Web. 1 Aug. 2017.
7. Daniel, Marie-Christine, and Didier Astruc. "Gold Nanoparticles: Assembly, Supramolecular Chemistry, Quantum-Size-Related Properties, And Applications Toward Biology, Catalysis, And Nanotechnology." *Chemical Reviews* 104.1 (2004): 293-346. Web. 28 July 2017.
8. Dykman, L. A., and N. G. Khlebtsov. "Gold nanoparticles in biology and medicine: recent advances and prospects." Acta Naturae (англоязычная версия) 3.2 (9) (2011) 34 – 55.
9. El-Saye, Mostafa A.; Huangab, Xiaohua "Gold nanoparticles: Optical properties and implementations in cancer diagnosis and photothermal therapy." Journal of Advanced Research (2010): 13-28.

10. El-Sayed, Mostafa A. "Some Interesting Properties Of Metals Confined In Time And Nanometer Space Of Different Shapes." *Accounts of Chemical Research* 34.4 (2001): 257-264. Web. 28 July 2017.
11. Frens, G. "Controlled Nucleation For The Regulation Of The Particle Size In Monodisperse Gold Suspensions." *Nature Physical Science* 241.105 (1973): 20-22. Web. 28 July 2017.
12. Ghosh, P et al. "Gold Nanoparticles In Delivery Applications☆." *Advanced Drug Delivery Reviews*60.11 (2008): 1307-1315. Web. 28 July 2017.
13. Gold Nanoparticles - Properties, Applications." AZoNano.com. N.p., 2017. Web. 19 Oct. 2017.
14. Gold Nanoparticles: Properties and Applications." Sigma-Aldrich. N.p., 2017. Web. 18 Oct. 2017.
15. Haiss, W. et al. "Determination of size and concentration of gold nanoparticles from UV− Vis spectra." *Analytical chemistry*79.11 (2007): 4215-4221.
16. Homola, Jiří. "Surface Plasmon Resonance Sensors For Detection Of Chemical And Biological Species." *Chemical Reviews* 108.2 (2008): 462-493. Web. 28 July 2017.
17. Hu, Jianqiang, Zhouping Wang and Jinghong Li. "Gold Nanoparticles With Special Shapes: Controlled Synthesis, Surface-enhanced Raman Scattering, and The Application in Biodetection." *Sensors* 7.12 (2007): 3299–3311. <https://www.ncbi.nlm.nih.gov/pmc/articles/PMC3841896/>.
18. Kesapragada, S. V. et al. "Nanospring Pressure Sensors Grown By Glancing Angle Deposition." *Nano Letters* 6.4 (2006): 854-857. Web. 1 Aug. 2017.
19. Kneipp, Katrin et al. "Single Molecule Detection Using Surface-Enhanced Raman Scattering (SERS)." *Physical Review Letters* 78.9 (1997): 1667-1670. Web. 28 July 2017.

20. Kong, Xiang Yang, and Zhong Lin Wang. "Spontaneous Polarization-Induced Nanohelixes, Nanosprings, And Nanorings Of Piezoelectric Nanobelts." *Nano Letters* 3.12 (2003): 1625-1631. Web. 1 Aug. 2017.
21. Link, Stephan, and Mostafa A. El-Sayed. "Size And Temperature Dependence Of The Plasmon Absorption Of Colloidal Gold Nanoparticles." *The Journal of Physical Chemistry B* 103.21 (1999): 4212-4217. Web. 28 July 2017.
22. Link, Stephan, and Mostafa A. El-Sayed. "Spectral Properties And Relaxation Dynamics Of Surface Plasmon Electronic Oscillations In Gold And Silver Nanodots And Nanorods." *The Journal of Physical Chemistry B* 103.40 (1999): 8410-8426. Web. 28 July 2017.
23. Martínez, J. C., et al. "Alternative metodology for gold nanoparticles diameter characterization using PCA technique and UV-Vis spectrophotometry." Nanoscience and Nanotechnology 2.6 (2012): 184-189.
24. McIlroy, D. N. et al. "Electronic And Dynamic Studies Of Boron Carbide Nanowires." *Physical Review B* 60.7 (1999): 4874-4879. Web. 1 Aug. 2017.
25. McIlroy, D. N. et al. "Nanosprings." *Applied Physics Letters* 79.10 (2001): 1540-1542. Web. 1 Aug. 2017.
26. McIlroy, David. "Integration of high surface area nanostructures into microreactors." 2015. Online. 11 October 2017. <http://imtb2015.fkit.hr/speakers/David%20McIlroy.pdf>.
27. Mueller, Michael R. *Fundamentals Of Quantum Chemistry*. New York: Kluwer Academic/Plenum Publishers, 2005. Print.

28. Njoki, Peter N. et al. "Size Correlation Of Optical And Spectroscopic Properties For Gold Nanoparticles." *The Journal of Physical Chemistry C* 111.40 (2007): 14664-14669. Web. 28 July 2017.

29. Njoki, Peter N. et al. "Aggregative Growth In The Size-Controlled Growth Of Monodispersed Gold Nanoparticles." *Langmuir* 26.16 (2010): 13622-13629. Web. 1 Aug. 2017.

30. Saha, Krishnendu et al. "Gold Nanoparticles In Chemical And Biological Sensing." *Chemical Reviews*112.5 (2012): 2739-2779. Web. 28 July 2017.

31. SEM: Scanning Electron Microscope A To Z. 1st ed. Tokyo, Japan: JEOL Inc, 2017. Web. 18 Oct. 2017.

32. Seney, Caryn S., Brittany M. Gutzman, and Russell H. Goddard. "Correlation Of Size And Surface-Enhanced Raman Scattering Activity Of Optical And Spectroscopic Properties For Silver Nanoparticles." *The Journal of Physical Chemistry C* 113.1 (2009): 74-80. Web. 1 Aug. 2017.

33. Sharma, Parvesh et al. "Nanoparticles For Bioimaging." *Advances in Colloid and Interface Science* 123-126 (2006): 471-485. Web.

34. Singh, J. P., et al. "Metal-coated Si springs: Nanoelectromechanical actuators." *Applied physics letters* 84.18 (2004): 3657-3659.

35. Sivapalan, Sean T. "STRUCTURAL AND PLASMONIC PROPERTIES OF GOLD NANOCRYSTALS." Ph.D. University of Illinois, 2013.p. 1-2.

36. Struve, Walter S. *Fundamentals Of Molecular Spectroscopy*. New York: J.Wiley, 1989. Print.

37. Thomas, Olivier, and C Burgess. *UV-Visible Spectrophotometry Of Water And Wastewater*. Amsterdam: Elsevier, 2007. Print.

38. Tomar, Avnika and Garima Garg. "Short Review on Application of Gold Nanoparticles." *Global Journal of Pharmacology* 7.1 (2013): 34-38.

39. Turkevich, J., Stevenson, P. C., Hillier, J. "A Study of the nucleation and growth processes in the synthesis of colloidal gold", Discussions of the Faraday Society, Vol. 11, 1951, pp. 55-75.

40. Wagner, R. S., and W. C. Ellis. "VAPOR-LIQUID-SOLID MECHANISM OF SINGLE CRYSTAL GROWTH." *Applied Physics Letters* 4.5 (1964): 89-90. Web. 1 Aug. 2017.

41. Wang, Lidong et al. "High Yield Synthesis And Lithography Of Silica-Based Nanospring Mats." *Nanotechnology* 17.11 (2006): S298-S303. Web. 1 Aug. 2017.

42. Wessel, John. "Surface-Enhanced Optical Microscopy." *Journal of the Optical Society of America B* 2.9 (1985): 1538. Web. 28 July 2017.

43. Wojcik, Peter M, et al. "Nucleation, evolution, and growth dynamics of armophous silica nanosprings." *Materials Research Express* 4 (2017): 1-10.

44. Wong, Ka Wai, et al. "Field-emission characteristics of SiC nanowires prepared by chemical-vapor deposition." *Applied Physics Letters* 75.19 (1999): 2918-2920.

45. Worner, Hans Jakob, and Frederic Merkt. "Fundamentals Of Electronic Spectroscopy." *Handbook Of High-Resolution Spectroscopy*. Martin Quack and Frederic Merkt. Hoboken, New Jersey: John Wiley & Sons, 2011. 175. Print.

46. Yguerabide, Juan, and Evangelina E. Yguerabide. "Light-Scattering Submicroscopic Particles As Highly Fluorescent Analogs And Their Use As Tracer Labels In Clinical And

Biological Applications." *Analytical Biochemistry* 262.2 (1998): 157-176. Web. 28 July 2017.

47. Zhang, D. et al. "Growth And Characterization Of Boron Carbide Nanowires." *Journal of Materials Science Letters* 18.5 (1999): 349-351. Web. 1 Aug. 2017.
48. Zhang, Daqing, et al. "Silicon Carbide Nanosprings." *Nano letters* 3.7 (2003): 983-987.
49. Zhang, Hai-Feng, et al. "Synthesis, Characterization, and manipulation of Helical SIO_2 Nanosprings." *Nano letter* (2003): 577-580. Document.
50. Zheng, Weitao. et al. "Light scattering and surface plasmons on small spherical particles." Light: Science & Applications (2014)
51. Zhou, Weilie, et al. "Fundamentals of scanning electron microscopy (SEM)." *Scanning microscopy for nanotechnology*. Springer New York, 2006. 1-40. Web. 6 June 2014

Appendix

General Information about Gold Nanoparticles:

Chemical Properties:

Chemical Data	
Chemical symbol	Au
CAS No.	7440-57-5
Group	11
Electronic configuration	[Xe] $4f^{142}$ $5d^{10}6s^{1}$

Physical Properties:

Properties	Metric	Imperial
Density	19.30 g/cm^3	0.697 lb/in^3
Molar mass	196.97 g/mol	-

Thermal Properties:

Properties	Metric	Imperial
Melting point	1064.43°C	1947.9741°F
Boiling point	2807°C	5084.6°F